International Journal of Heat and Mass Transfer 215 (2023) 124479

Contents lists available at ScienceDirect

International Journal of Heat and Mass Transfer

journal homepage: www.elsevier.com/locate/ijhmt

Droplets bouncing on rotating curved surfaces with elevated temperatures

Chuchen Yue [1], Qingwen Dai [1,*], Wei Huang, Xiaolei Wang

College of Mechanical and Electrical Engineering, Nanjing University of Aeronautics & Astronautics, Nanjing 210016, China

ARTICLE INFO

Keywords:
Droplet impact
Bouncing
Rotating curved surfaces
Oil film
Temperature effect

ABSTRACT

In this work, droplets bouncing on curved surfaces with elevated temperatures are reported. The bouncing and depositing phenomena of different lubricant droplets are confirmed. The influence of initial diameter, tangential velocity, and surface roughness on the impact dynamics of silicone oil droplets on wetted curved surfaces is investigated, and the temperature dependence of the bouncing phenomenon is highlighted. Bouncing and depositing thresholds under various conditions are summarized. It is found that surface roughness has the most significant negative effect on the bounceable velocity range, followed by initial diameter and tangential velocity. A theoretical model and force analysis are established to explain the bouncing mechanism. The modified Bond numbers and Ohnesorge numbers are introduced to predict the bouncing thresholds. This work provides sufficient experimental and theoretical insights into manipulating droplets bouncing on wetted and curved surfaces with elevated temperatures.

1. Introduction

Droplet impacting phenomena widely exist in nature and industrial applications such as inkjet printing [1], self-cleaning [2], anti-icing [3], spray cooling [4], etc. Making droplets bounce has attracted considerable attention since many interfacial properties are directly related to that, for example, heat transfer efficiency [5].

Since superhydrophobic surfaces have relatively low surface energy, on which droplets can easily bounce off, extensive studies have been conducted on this aspect including constructing micro-nano structures [6] and low surface energy coatings [7,8] to control the contact time before droplets bouncing [9]. In another aspect, coating a solid surface via a liquid film can also reduce its surface energy, and investigations have revealed that water droplets can bounce off wetted flat solid surfaces [10], or even liquid pool [11] since the flowing air film between droplets and the liquid film provides a lifting force for bouncing [10,12,13]. Besides, the vapor generated by the evaporation of droplets when impacting hot surfaces can also promote bouncing [14], which is manifested as the famous Leeidenforst phenomenon [15].

Droplets bouncing dynamics become complex once the surface is curved [16]. Due to the existence of surface curvature, the symmetry and bouncing direction of droplets were changed directly [17,18]. Moreover, the influence of geometric dimension [19] and viscosity [20] of droplets also play a key role. Note that these studies were carried out at room temperature, as the physicochemical properties of the liquid are temperature-dependence, here come some basic questions, what would happen if curved surfaces are heated? Will droplets bounce again or not? A review of the open literature about this aspect is currently lacking. Revealing the temperature dependency of droplets bouncing on curved surfaces is of great significance for many applications. For instance, in the mist lubrication system [21], rotating shafts service under an extreme temperature range, where oil droplets bouncing or depositing on them would extremely affect the lubrication and heat transfer efficiency [22].

In our previous work [23], silicone oil droplets impacting rotating cylinders were investigated. However, the temperature effect of the cylinder was not considered, which is more common in real working conditions. Herein, in this work, oil droplets bouncing on curved surfaces with elevated temperatures are investigated. The bouncing and depositing phenomenon of different oil droplets on wetted curved surfaces is confirmed, and the corresponding limitations under various conditions are highlighted. A physical model is established to explain the bouncing mechanism, and dimensionless parameters of Bond number and Ohnesorge number are evolved to reveal the physical essence. The prediction of the bouncing threshold is consistent with the experimental results. This work provides sufficient experimental and theoretical insights into manipulating droplets bouncing on wetted curved surfaces with elevated temperatures.

* Corresponding author.
E-mail address: daiqingwen@nuaa.edu.cn (Q. Dai).
[1] These authors contributed equally to this work.

https://doi.org/10.1016/j.ijheatmasstransfer.2023.124479
Received 6 April 2023; Received in revised form 23 June 2023; Accepted 3 July 2023
Available online 27 July 2023

2. Materials and methods

2.1. Materials

All curved surfaces (cylinders) are made of 304 stainless steel with a radius of curvature R_ρ=5 mm, axial length L = 20 mm, and surface roughness Sa=0.3, 1.5, 3.3, and 6.7 μm, respectively. Differ from the dimensionless number described in the literature [24,25], the surface roughness is obtained by a three-dimensional optical profiler (ContourGT-K, Bruker), and the measuring processes are as follows: scanning the entire profile of the cylinder, flattening the surface, and then the surface roughness is calculated as same as that on planes, which is the average of the absolute value of the difference in height of each point relative to the average surface. Lubricants of polyalphaolefin (abbreviated as PAO4, viscosity μ=0.02 Pa·s, and surface tension γ=31 mN/m), olive oil (μ=0.1 Pa·s and γ=33 mN/m), paraffin oil (μ=0.03 Pa·s and γ = 30 mN/m), and silicone oil (μ = 0.1 Pa·s and γ = 21 mN/m) were adopted. They were purchased from Sinopec Yangzi Petrochemical Company of China with a purity of >95% and used as received. The contact angle of silicone oil on cylinders with different Sa is measured and shown in Fig. 1b, thus, the Wenzel wetting regime holds.

2.2. Methods

The initial diameter D_0=1.6, 1.8, 2.2, and 2.5 mm and impact velocity V of droplets were controlled by the diameter of the microsyringe needle and its initial height, respectively. All tested surfaces were prewetted before the droplet impact experiments. Fig. 1a shows the prewetting progress. By setting the temperature of the curved surface to a specific value of 0, 20, 60, and 100 °C (via placing the curved surface on a copper base which placed on a temperature control platform, K-type thermocouples were used to confirm the temperature with an accuracy of ±1.5 °C), droplets with a specific volume were released on the rotating surface (controlled by a motor with an angular velocity ω=50 rad/s) successively after separating the surface from the base. Then, a uniform liquid film would be formed on the cylinder within 30 s, and the film thickness h can be calculated as

$$h = \sqrt{\frac{Volume}{\pi L} + R_\rho^2} + R_\rho \tag{1}$$

As the uniform oil film was formed, a droplet was injected on the surface, and the whole impact process was recorded by a high-speed camera (i-SPEED 726R, iX Cameras, UK) and analyzed by image processing software, respectively.

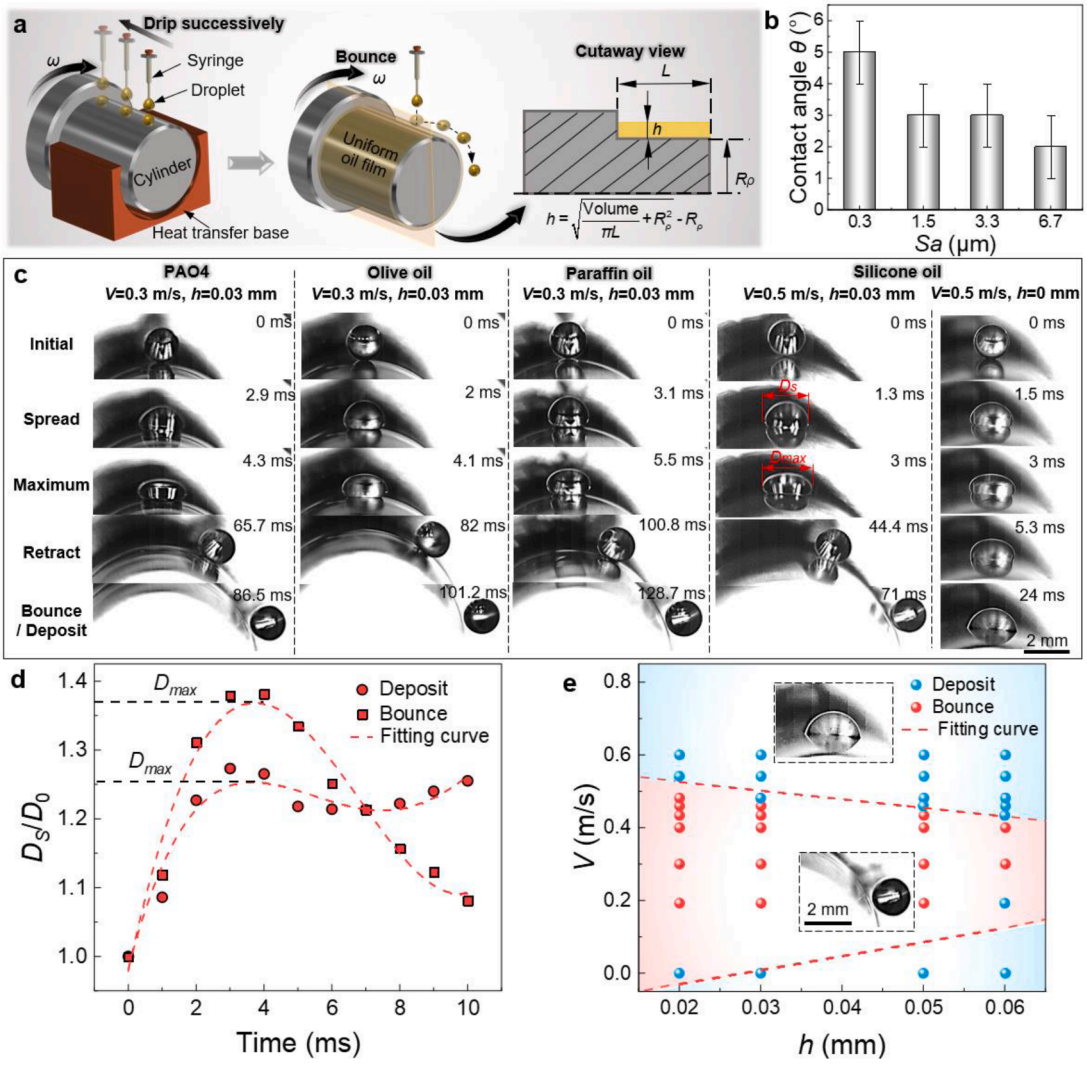

Fig. 1. Experimental procedure and basic impacting dynamics. (**a**) Schematic diagram of the experimental setup and method of generating an oil film and calculating film thickness. (**b**) The contact angle of silicone oil (volume=2 mm^3, μ=0.1 Pa·s) on cylinders with different Sa at T = 20 °C. (**c**) Comparison of four lubricant droplets impacting on a static surface. (**d**) Changing progress of D_s/D_0 of the silicone oil droplets in Fig. 1c, where the condition of the red circle is V = 0.5 m/s and h = 0 mm and the red rectangle is V = 0.5 m/s and h = 0.03 mm. (**e**) Relationship between the bounceable velocity range and h.

3. Results and discussion

3.1. Basic bouncing dynamics

Fig. 1c shows the typical impact dynamics of four lubricant droplets on a static surface with $T = 20$ °C and Sa=0.3 μm, where spread, maximum, retract, bounce, and deposit processes are included, as well as a comparison between dry and wetted surfaces. As the object for droplets impacting is the oil film, it is not necessary to apply the wetting regime. Fig. 1d exhibits the corresponding change progress of the ratio of spreading diameter D_s and D_0 with elapsed time. It can be seen that the maximum spread diameter D_{max} and the retraction time of the bouncing droplet are both larger than the deposit one, which is attributed to the lubrication effect of air film [26]. To determine the best experimental oil film thickness, different film thicknesses of $h = 0.02$, 0.03, 0.05, and 0.06 mm were compared. As shown in Fig. 1e, under a specific oil film thickness h (for example $h = 0.02$ mm), droplets undergo a process of depositing, bouncing, and depositing again with increasing impact velocity, and the corresponding depositing and bouncing impact velocity regions were identified by blue and red color, respectively. With increasing h, different depositing and bouncing regions were obtained. It can be seen that the bounceable velocity range (red area) exhibits a negative correction with h. Since the range is narrow with a higher h while the oil film takes longer to reach uniformity with a lower h, $h =$ 0.03 mm was chosen in this work. Considering the wide application of silicone oil in industry, it was adopted in the following sections, and the statistical scattering of the reported results are similar to that shown in Fig. 1e.

3.2. Initial diameter D_0

Fig. 2a shows the increase of D_0 and T inhibits droplets bounce off the static surface. It can be seen from Fig. 2b–e that the minimum and maximum bounceable velocities V_{lower} and V_{upper} (the lower and upper fitting curves, respectively) are both positively correlated with D_0 at the same T. All bounceable velocity ranges (areas between two red lines) are approximately negatively correlated with D_0, but the influence of T is nonlinear, with the range experienced the evolution of increasing (from 0 to 20 °C), decreasing (from 20 to 60 °C), and increasing (from 60 to 100 °C). Initial diameter plays a significant influence on the gravity F_g and the inertial force F_i of droplets [27], which can be written as [28, 29]:

$$\begin{cases} F_g = \dfrac{\pi \rho g D_0^3}{6} \\ F_i = \dfrac{\pi \rho D_0^2 V^2}{6} \end{cases} \tag{2}$$

where g is the gravity acceleration. According to the capillary length $l_c=(\gamma(T)/\rho g)^{1/2} \approx 1.35 \sim 1.5$ mm, the gravity cannot be ignored. Therefore, the increasing of D_0 leads to a larger gravity and inertial force, which weakens the support of the air film in the vertical direction and results in depositing.

3.3. Tangential velocity v_t

The major distinction between static and rotating curved surfaces is the tangential force [30]. A unique impact phenomenon exists when droplets impact the wetted and rotating surface, i.e., there is no displacement difference on the left side during spreading (2.2 ms) and reaching D_{max} (3.6 ms) with the direction of V_t is right, as shown in Fig. 3a. Compared with the right side, the left spreading front will be subjected to a larger aerodynamic force [29]:

$$F_{af} \sim \rho_a V_t^2 D_0^2 \tag{3}$$

whose scale is 0.1–1 μN and ρ_a=1.2 kg/m^3 is the air density. As the droplet keeps spreading under the action of F_g and F_i, the displacement generated by the leftward spreading and the rightward rotation cancel each other so that the left side remains essentially static. Due to the high viscosity and poor fluidity, it was challenging to obtain a uniform oil film when wetting the rotating surface with a high V_t and low T, which is why droplets fail to bounce under the condition of V_t=0.75 m/s, and $T =$ 0 ° C in Fig. 3b. The slope of both V_{lower} and V_{upper} change from negative to positive that demonstrating temperature has a stronger effect on larger diameter droplets. Similar to Figs. 2b–e, the bounceable velocity range experienced the evolution of increasing (from 0 to 20 °C), decreasing (from 20 to 60 °C), and increasing (from 60 to 100 °C).

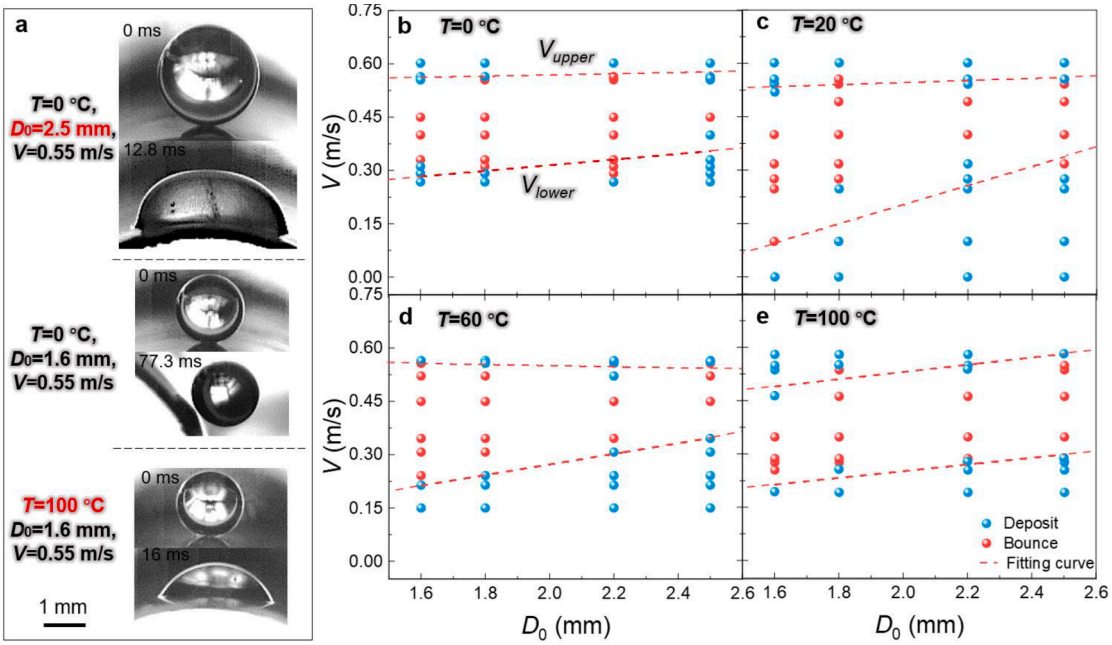

Fig. 2. Effect of initial diameter on droplet impacting. (**a**) Typical depositing and bouncing phenomenon under different conditions. (**b**)–(**e**) Relationship between the bounceable velocity range and the initial diameter with elevated temperatures.

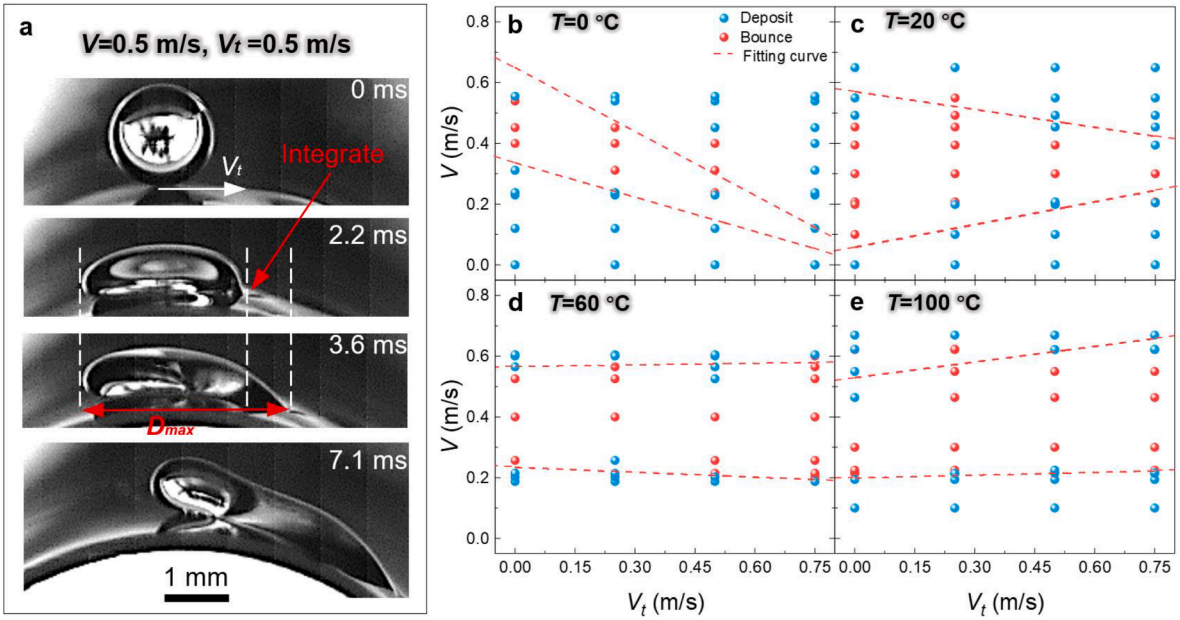

Fig. 3. Effect of tangential velocity on droplet impacting. (**a**) Relative static spreading that is dominated by inertia. (**b**)–(**e**) Relationship between the bounceable velocity range and tangential velocity with elevated temperatures.

3.4. Surface roughness Sa

Fig. 4a–d shows the influence of surface roughness on the bouncing dynamic. It is difficult to bounce on the wetted and static rough surface and bounceable velocity ranges are negatively correlated with *Sa*, but V_{lower} is very sensitive to *T*. To illustrate the roughness effect, the wetting condition of curved surfaces with *Sa*=0.3 and 6.7 μm are shown in Fig. 4e. It can be seen that most of the oil film is used to fill the grooves of the rough surface so that there is a continuous wavy shape rather than leveling. Therefore, it leads to the obvious differences in the bounceable velocity range between smooth and rough surfaces, which is 0 ~ 0.49 m/s and 0.39 ~ 0.45 m/s under $T = 20$ °C, respectively. Referring to the data shown in Fig. 1b, the amplitude of the contact angle is quite low, thus, it has a limited effect on the spreading process. Moreover, the oil droplets are impacting onto the oil film, which furthermore diminishes the effect of the apparent contact angle.

3.5. Bouncing and depositing thresholds

To present intuitive results on the dominance of *T*, D_0, *Sa*, and V_t over the impact dynamics of droplets, 3D color maps are plotted to exhibit the bounceable velocity range (the space between V_{lower} and V_{upper}), as shown in Fig. 5a–c. It can be seen that the bounceable velocity range is smallest at a low *T* and large D_0, while a smaller D_0 corresponds to an overall larger range. The increasing of *T* and V_t at the same time promotes droplet bouncing, but the combined effects of low *T* and high V_t can be fatal. Obviously, a higher *Sa* largely inhibits the range of droplets bouncing, regardless of temperature. Therefore, *Sa* has the greatest

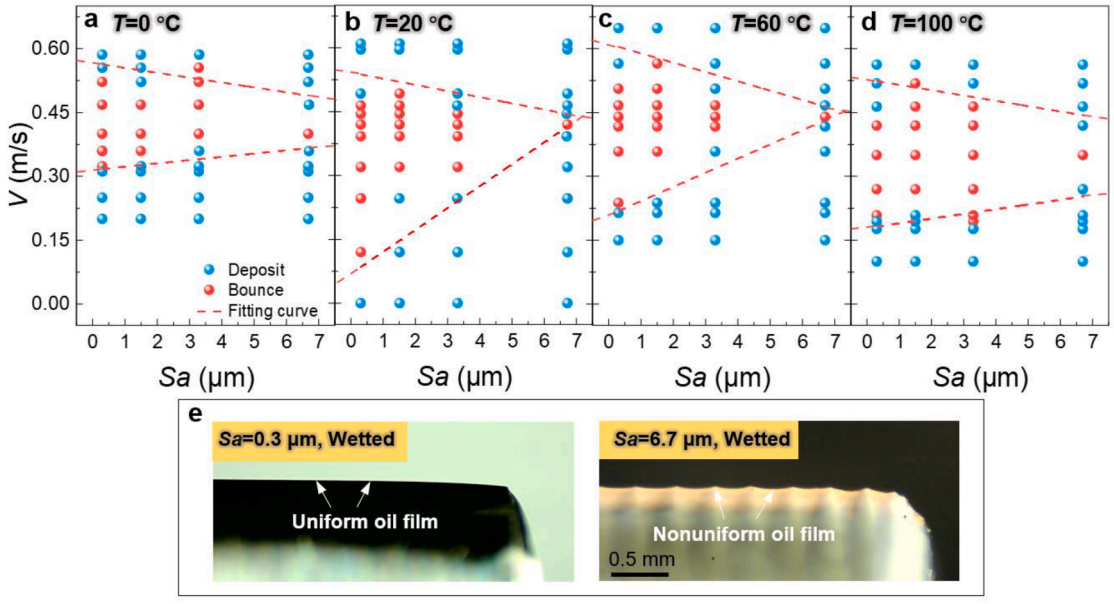

Fig. 4. Effect of surface tension on droplet impacting. (**a**) ~ (**d**) Relationship between the bounceable velocity range and surface roughness with elevated temperatures. (**e**) Comparison of the wetting condition between smooth and rough curved surfaces.

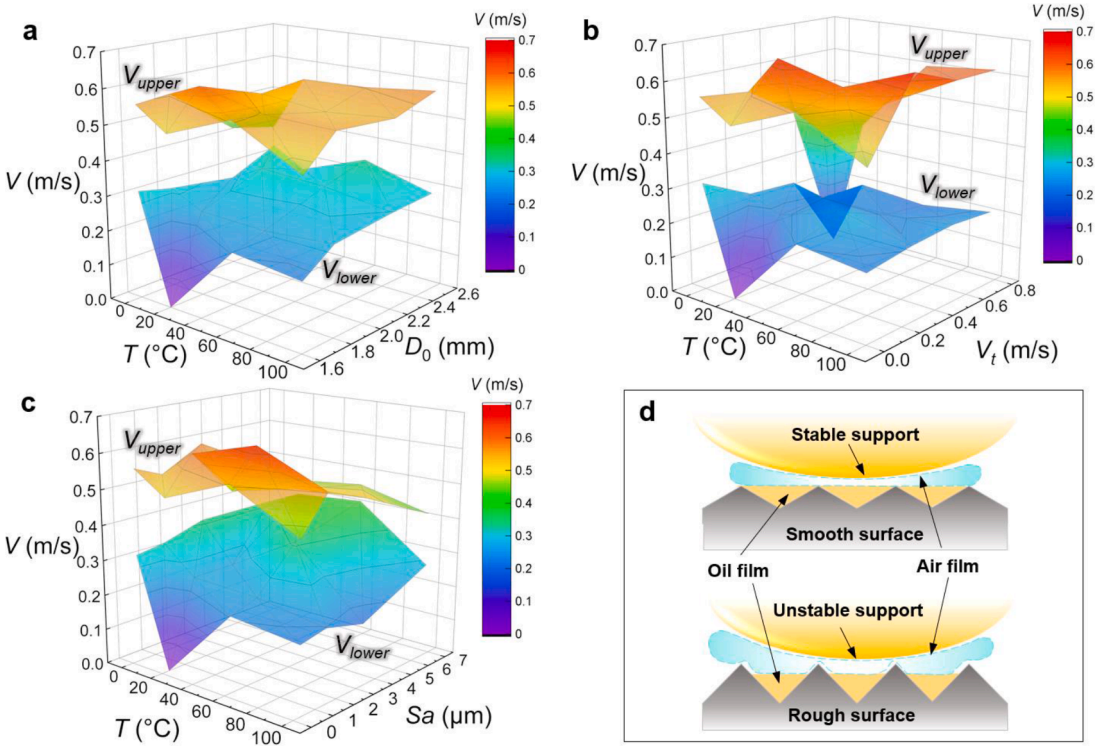

Fig. 5. Droplet bounceable ranges and the effect of surface roughness on air film. (**a**)–(**c**) 3D color maps of V_{lower} and V_{upper}. (**d**) Model of the wetting conditions on smooth and rough surfaces.

influence on V_{lower} and V_{upper} followed by V_t and D_0 with all T from 0 to 100 °C.

The above results can be interpreted as follows. For the investigated droplets in this work, the Bond number $Bo=\rho g R_0^2/\gamma(T)$ (R_0 is the initial radius [31]) scales as 0.1, according to Eq. 2, the increasing of Bo from 0.28 to 0.7 (as D_0 increases from 1.6 to 2.5 mm) greatly enhanced the magnitude of F_g (from 20 to 77 μN) and F_i (from 0.4 to 0.95 mN), resulting in the difficulty in bouncing and a reduction in the bounceable velocity range. Meanwhile, the viscosity and surface tension of liquids decreases with the increasing temperature [$\mu(T)=\mu(T_0)e^{-0.018(T-T_0)}$ and $\gamma(T)=\gamma(T_0)-0.05(T-T_0)$, where $\mu(T_0)$ and $\gamma(T_0)$ represent the viscosity and surface tension at the reference temperature T_0=20 °C] [27,32], the viscous resistance during spreading would be reduced when T rises from 0 to 100 °C, which means the lower internal friction between molecules

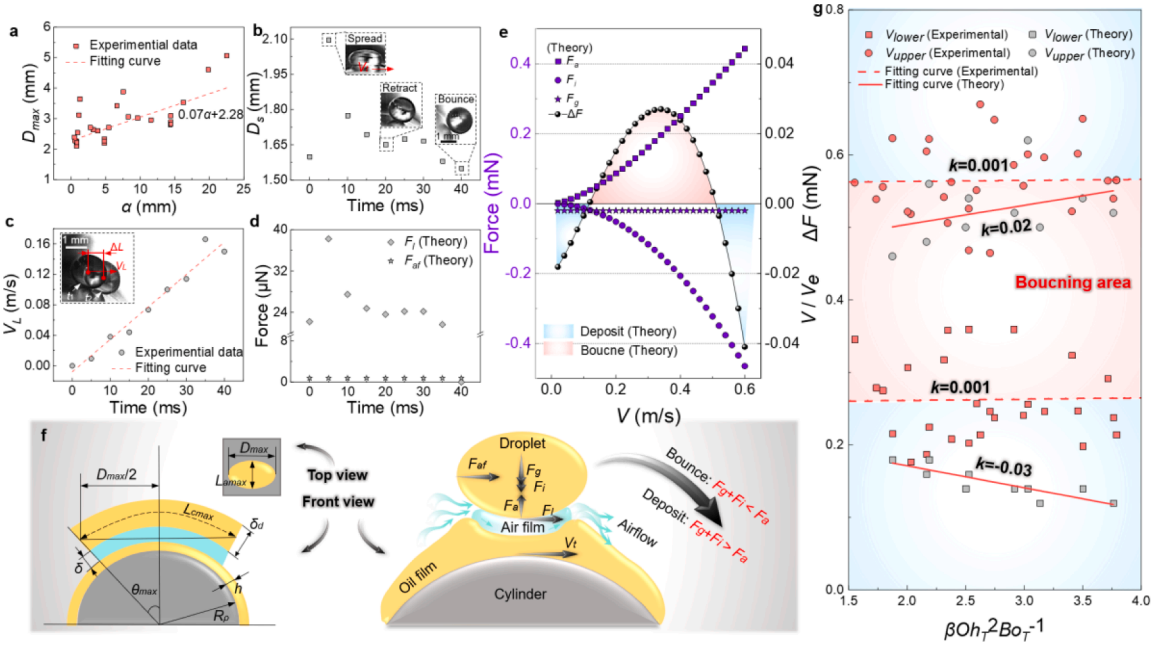

Fig. 6. Forces in the horizontal and vertical directions, theoretical models, and data fitting. (**a**) Relationship between D_{max} and α. (**b**)–(**d**) Evolution of D_s, V_L, F_i, and F_{af}. (**e**) The evolution of ΔF, F_i, F_g, and F_a. (f) 2D maximum spreading model and force analysis model. (**g**) Relationship between V_{upper}, V_{lower}, and β obtained by theory and experiments.

promotes the deformation of droplets and makes it pierce the air layer, but too low a temperature can make it difficult to even out the oil film and affect bouncing [20]. Therefore, increasing T when T is low can reduce γ and μ which allows droplets to bounce, but the excessive T will make droplets deposit, thus there is a general trend of increasing and then decreasing of the bounceable velocity range with increasing T. Since a uniform oil film can be formed on the smooth surface, the compressed air film could provide stable support for droplets, but the existence of grooves between microstructures makes it distributes non-uniformly on the rough one that pierces the air film [33,34], as shown in Fig. 5d.

3.6. Theoretical model and prediction

To quantify the impact progress, Fig. 6f shows a 2D maximum spreading model and force analysis model. As the droplet is approximately a curved oval cake when reaching D_{max}, taking L_{cmax} and L_{amax} as the maximum length of the horizontal and axial positions [35], which can be defined as

$$L_{cmax} = (\delta_d + 2h + 2\delta + 2R_\rho)\theta_{max},\ L_{amax} = \frac{10L_{cmax}}{11} \tag{4}$$

where $\delta_d \sim 4R_0^3/{D_{max}}^2$ is the thickness of the droplet [8], R_0=D_0/2, $\delta \sim R_0 St^{-2/3}$ is the thickness of the air film, in which dimensionless number St=$\rho V R_0/\mu_a$ is the Stokes number that scales as 100 ~ 10,000 where μ_a=18×10^{-6} Pa·s is the viscosity of air [12]. θ_{max} is the maximum spreading angle on one side, which can be calculated as

$$\theta_{max} = \arcsin\left(\frac{D_{max}}{\delta_d + 2h + 2\delta + 2R_\rho}\right) \tag{5}$$

since D_{max} is influenced by D_0, Sa, V_t, and T, a composite parameter α is introduced with D_0=1.6 ~ 2.5 mm, Sa=0.3 ~ 6.7 μm, V_t=0 ~ 0.75 m/s, T = 0–100 °C, and V = 0.5–1.5 m/s, which is defined as

$$\alpha = \frac{D_0^2}{(D_0 + Sa)}\left(\frac{V}{V_e + V_t}\right)\left(1 + \frac{T}{T_0}\right) \tag{6}$$

where V_e=1 m/s is the unit velocity and α scales as 0 ~ 10 mm. It can be seen from Fig. 6a that D_{max} can be defined as

$$D_{max} = \frac{7D_0^2}{100(D_0 + Sa)}\left(\frac{V}{V_e + V_t}\right)\left(1 + \frac{T}{T_0}\right) + 2.28 \tag{7}$$

In the horizontal direction, aerodynamic force F_{af} generated by the airflow and the lubricant force F_l will form a rightward thrust for droplets with the wetted cylinder rotates clockwisely [13], where

$$F_l \sim \frac{\mu_a V_t D_{max}^2}{\delta} \tag{8}$$

In the vertical direction, the droplet is deformed by F_g and F_i, which are countered by the support forces F_a that generated by the air film, while the relative pressure ΔP is estimated by Laplace's equation [11,18]

$$\Delta P \sim \gamma(T)\left(\frac{2}{L_{com}} + \frac{2}{\delta}\right),\ F_a = S\Delta P \tag{9}$$

where L_{com} =($L_{amax}{L_{cmax}}^2$)$^{1/3}$ is the equivalent diameter of the droplet [17], and S=$\pi R_\rho \theta_{max} L_{amax}$/2 is the contact area between the bottom of the droplet and the air film [35]. Since ΔP lacks precision, F_a can be corrected within the parameters of this experiment as

$$F_a = \pi R_\rho \theta_{max} L_{amax} \gamma(T)\left(\frac{1}{L_{com}} + \frac{1}{\delta}\right)\tan\left(\frac{6V}{5V_e}\right)^{\left(1.4 - \frac{V}{V_e}\right)} \tag{10}$$

Therefore, the bounceable condition in this model is

$$\begin{cases} \Delta F = F_a - F_g - F_i > 0 & (Bouncing) \\ \Delta F = F_a - F_g - F_i < 0 & (Depositing) \end{cases} \tag{11}$$

Let's take the condition of V = 0.5 m/s, T = 0 °C, V_t=0.5 m/s, Sa=0.3 μm, and D_0=1.6 mm as an example to illustrate the change in F_l and F_{af} during impacting. Fig. 6b shows the evolution of D_s with time which prepares data for calculating F_l, and the average horizontal velocity V_L can be got by calculating the displacement difference ΔL of the droplet center at t_1 and t_2, i.e.,

$$V_L = \Delta L/(t_2 - t_1) \tag{12}$$

Due to the influence of inertia, V_L increases slightly in the spreading stage. With the enhanced influence of gravity on vertical motion, the droplet slides rapidly, resulting in a continuous rising of V_L. When the droplet starts to bounce off at 40 ms, V_L plunges by the loss of lubricating force, as shown in Fig. 6c. Fig. 6d presents the evolution of F_l and F_{af}, which highlightings the close correlation between F_l and D_s.

To visualize the forces on droplets in the vertical direction at different V and the corresponding impacting dynamics, Fig. 6e shows the evolution of F_g, F_i, F_a, and ΔF with V = 0.02–0.6 m/s, T = 0 °C, V_t=0.5 m/s, Sa=0.3 μm, and D_0=1.6 mm when droplets reach D_{max}. It is clear that F_g plays a dominant role at V = 0.02–0.1 m/s, while F_g, F_i, and F_a are of the same magnitude at V = 0.1–0.28 m/s, and it becomes the contest between F_i and F_a at V = 0.28–0.6 m/s. Hence, ΔF keeps less than 0 until V = 0.12 m/s, and then F_a starts to be stronger than the downward combined force of F_g and F_i but it loses the dominance when V = 0.52 m/s.

To fully consider the effect of the parameters discussed above on the bouncing dynamics of droplets and combine theoretical calculations to verify the reliability of experimental results, dimensionless numbers β, Bo, and Ohnesorge number Oh=$\mu/(\rho D_0 \gamma)^{1/2}$ that relates the viscous to inertial forces and the surface tension force are combined and used to characterize V_{lower} and V_{upper}. The scale of β is 1 and it is composed of D_0, Sa, V_e, and V_t

$$\beta = \frac{V_e D_0}{Sa^{1/5}(V_e + V_t)} \tag{13}$$

as γ and μ is the function of T, the expressions of Oh and Bo can be modified as

$$\begin{cases} Oh_T = \dfrac{\mu(T_0)e^{-0.018(T-T_0)}}{\sqrt{\rho D_0(\gamma(T_0) - 0.05(T - T_0))}} \\ Bo_T = \dfrac{\rho g R_0^2}{\gamma(T_0) - 0.05(T - T_0)} \end{cases} \tag{14}$$

where both scales of Oh_T and Bo_T are 0.1, so the function relationship between dimensionless number V/V_e and β, Bo_T, and Oh_T is

$$VV_e^{-1} \sim \beta Oh_T^2 Bo_T^{-1} \tag{15}$$

All experiments are limited with V_t=0–0.75 m/s, Sa=0.3–6.7 μm, T = 0–100 °C, and D_0=1.6–2.5 mm, while the theory calculation conditions are V_t=0.25–0.75 m/s, Sa=0.3–6.7 μm, T = 0–100 °C, and D_0=1.6 mm. It can be seen from Fig. 6g that the dotted red lines are the fitting curve of the red circle and red rectangle obtained by experiments, while the solid red lines correspond to the gray circle and gray rectangle obtained by theory. The bounceable velocity range (red area) is less influenced by the horizontal coordinate for experiments with the slope k of the upper and lower fitted curves are k = 0.001 and k = 0.001, respectively, but it exhibits a positive correlation with the horizontal coordinate for theory with k of the upper and lower fitted curves are k = 0.02 and k=−0.03, respectively.

The reason why droplets can bounce on wetted surfaces is the existence of the air film between droplets and the liquid film provides support for droplets [23]. At low V, the pressure of the air film is not strong enough to support droplets, while high V leads to increases in the

deformation of droplets and liquid film, resulting in depositing. So, there is a velocity range that is suitable for droplet bouncing, just like the red area in Fig. 6g. Since Oh_T represents the effect of viscous forces on droplets, the increase of Oh_T leads to the increasing friction between the molecules within droplets, and a large amount of initial energy will be used to overcome viscous resistance during spreading, resulting in a reduced degree of deformation and a relatively stable support area of the air film, which is conducive to droplet bouncing. The competition between gravity, inertia force, and the support of the air film is the decisive factor in determining droplet bouncing. After increasing Bo_T, the support force is gradually being put at a disadvantage. Therefore, there is a positive correlation between V/V_e and Oh_T, while a negative one is between V/V_e and Bo_T, and the best bounceable velocity is 0.26–0.56 m/s with T = 0–100 °C. However, only the effects of T on μ and γ were considered in experiments, while that on density, air pressure, and other relevant factors need to be investigated in the future.

4. Conclusion

In this work, we have experimentally and theoretically investigated silicone oil droplets bounce off wetted curved surfaces with elevated temperatures. Comparison of the impact of four lubricant droplets demonstrates the universality of bouncing. Bouncing and depositing thresholds under various conditions are highlighted. It is found that surface roughness has the greatest negative influence on the bounceable velocity range, followed by tangential velocity and initial diameter. The increase in droplet diameter leads to an increase in gravity and inertial force, reducing the likelihood of droplets bouncing. The existence of tangential velocity leads to a special relative static spreading that is dominated by inertia. Increasing surface roughness will make the oil film distributes nonuniformly, resulting in unstable support of the air film and droplets depositing. Theoretical model and force analysis were established to explain the bouncing mechanism, and an example analysis demonstrated the relationship between force and spreading. A dimensionless impact factor β and modified Bond number Bo_T and Ohnesorge numbers Oh_T were combined to illustrate the velocity threshold of bouncing and depositing, where there was $VV_e^{-1} \sim \beta Oh_T^2 Bo_T^{-1}$. The theoretical predictions are in good agreement with the experimental results, and the negative effects of rising Bond number and temperature on bouncing were elucidated, which increases the gravity and inertial force and decreases the viscosity and surface tension, respectively. The critical conditions of droplets bouncing and depositing on wetted curved surfaces provide a design concept for modern lubrication systems.

CRediT authorship contribution statement

Chuchen Yue: Investigation, Methodology, Writing – original draft, Writing – review & editing. **Qingwen Dai:** Conceptualization, Funding acquisition, Writing – review & editing. **Wei Huang:** Methodology, Project administration. **Xiaolei Wang:** Supervision.

Declaration of Competing Interest

The authors declare that they have no known competing financial interests or personal relationships that could have appeared to influence the work reported in this paper.

Data availability

Data will be made available on request.

Acknowledgments

The authors (Q.D., C.Y., W.H., and X.W.) are grateful for the support from the National Natural Science Foundation of China (Grant No. 51805252); Q.D. acknowledges the support from the Alexander von Humboldt Foundation.

References

[1] T.M. Schutzius, S. Jung, T. Maitra, G. Graeber, M. Köhme, D. Poulikakos, Spontaneous droplet trampolining on rigid superhydrophobic surfaces, Nature 527 (7576) (2015) 82–85, https://doi.org/10.1038/nature15738.
[2] Y. Lu, S. Sathasivam, J. Song, C.R. Crick, C.J. Carmalt, I.P. Parkin, Robust self-cleaning surfaces that function when exposed to either air or oil, Science 347 (6226) (2015) 1132–1135, https://doi.org/10.1126/science.aaa0946.
[3] X. Deng, L. Mammen, H.J. Butt, D. Vollmer, Candle soot as a template for a transparent robust superamphiphobic coating, Science 335 (6064) (2012) 67–70, https://doi.org/10.1126/science.1207115.
[4] X. Zhao, B. Zhang, X. Xi, Z. Yin, Analysis and prediction of single-phase and two-phase cooling characteristics of intermittent sprays, Int. J. Heat Mass Transf. 133 (2019) 619–630, https://doi.org/10.1016/j.ijheatmasstransfer.2018.12.146.
[5] J. Li, Y. Hou, Y. Liu, C. Hao, M. Li, M.K. Chaudhury, S. Yao, Z. Wang, Directional transport of high-temperature Janus droplets mediated by structural topography, Nat. Phys. 12 (6) (2016) 606–612, https://doi.org/10.1038/nphys3643.
[6] Y. Liu, L. Moevius, X. Xu, T. Qian, J.M. Yeomans, Z. Wang, Pancake bouncing on superhydrophobic surfaces, Nat. Phys. 10 (7) (2014) 515–519, https://doi.org/10.1038/nphys2980.
[7] S. Chen, Q. Dai, X. Yang, J. Liu, W. Huang, X. Wang, Bioinspired functional structures for lubricant control at surfaces and interfaces: wedged-groove with oriented capillary patterns, ACS Appl. Mater. Interfaces 14 (37) (2022) 42635–42644, https://doi.org/10.1021/acsami.2c09439.
[8] M. Abolghasemibizaki, R.L. McMasters, R. Mohammadi, Towards the shortest possible contact time: droplet impact on cylindrical superhydrophobic surfaces structured with macro-scale features, J. Colloid Interface Sci. 521 (2018) 17–23, https://doi.org/10.1016/j.jcis.2018.03.005.
[9] H. Wang, C. Liu, H. Zhan, Y. Liu, Droplet asymmetric bouncing on inclined superhydrophobic surfaces, ACS Omega 4 (7) (2019) 12238–12243, https://doi.org/10.1021/acsomega.9b01348.
[10] M. Muschi, B. Brudieu, J. Teisseire, A. Sauret, Drop impact dynamics on slippery liquid-infused porous surfaces: influence of oil thickness, Soft Matter 14 (7) (2018) 1100, https://doi.org/10.1039/C7SM02026K.
[11] Z. Che, A. Deygas, O.K. Matar, Impact of droplets on inclined flowing liquid films, Phys. Rev. E 92 (2) (2015), 023032, https://doi.org/10.1103/PhysRevE.92.023032.
[12] N.P. Thrivikraman, A. Khare, A.S. Hegde, A.R. Harikrishnan, Confined evaporation-mediated enhanced residence time of levitated water drops over deep oil pools, Langmuir 37 (49) (2021) 14472–14482, https://doi.org/10.1021/acs.langmuir.1c02443.
[13] T. Tran, E.J. Staat, A. Susarrey-Arce, T. Fortsch, A. Houselt, H. Gardeniers, A. Prosperetti, D. Lohse, C. Sun, Droplet impact on superheated micro-structured surfaces, Soft Matter 9 (2013) 3272–3282, https://doi.org/10.1039/C3SM27643K.
[14] C. Kuhn, D. Schweigert, C. Kuntz, M. Börnhorst, Single droplet impingement of urea water solution on heated porous surfaces, Int. J. Heat Mass Transf. 181 (2021), 121836, https://doi.org/10.1016/j.ijheatmasstransfer.2021.121836.
[15] M.A.J. van Limbeek, M.H. Klein Schaarsberg, B. Sobac, A. Rednikov, C. Sun, P. Colinet, D. Lohse, Leidenfrost drops cooling surfaces: theory and interferometric measurement, J. Fluid Mech. 827 (2017) 614–639, https://doi.org/10.1017/jfm.2017.425.
[16] Y. Wang, Y. Wang, S. Wang, Droplet impact on cylindrical surfaces: effects of surface wettability, initial impact velocity, and cylinder size, J. Colloid Interface Sci. 578 (2020) 207–217, https://doi.org/10.1016/j.jcis.2020.06.004.
[17] G. Liang, Y. Guo, Y. Yang, S. Guo, S. Shen, Special phenomena from a single liquid drop impact on wetted cylindrical surfaces, Exp. Therm. Fluid Sci. 51 (2013) 18–27, https://doi.org/10.1016/j.expthermflusci.2013.06.012.
[18] T. Gilet, J.W.M. Bush, Droplets bouncing on a wet, inclined surface, Phys. Fluids 24 (12) (2012), 122103, https://doi.org/10.1063/1.4771605.
[19] R.N. Valani, A.C. Slim, T. Simula, Superwalking droplets, Phys. Rev. Lett. 123 (2) (2019), 024503, https://doi.org/10.1103/PhysRevLett.123.024503.
[20] G. Liang, Y. Yang, Y. Guo, N. Zhen, S. Shen, Rebound and spreading during a drop impact on wetted cylinders, Exp. Therm. Fluid Sci. 52 (2014) 97–103, https://doi.org/10.1016/j.expthermflusci.2013.09.001.
[21] Y. Zama, Y. Odawara, T. Furuhata, Experimental investigation on velocity inside a diesel spray after impingement on a wall, Fuel 203 (2017) 757–763, https://doi.org/10.1016/j.fuel.2017.04.099.
[22] Y. Pei, J. Qin, X. Li, D. Zhang, K. Wang, Y. Liu, Experimental investigation on free and impingement spray fueled with methanol, ethanol, isooctane, TRF and gasoline, Fuel 208 (2017) 174–183, https://doi.org/10.1016/j.ijmultiphaseflow.2021.103774.
[23] Q. Dai, C. Yue, W. Huang, X. Wang, Droplets impact on rotating cylinders, Chem. Eng. Sci. 273 (1) (2023), 118669, https://doi.org/10.1016/j.ces.2023.118669.
[24] E. Bormashenko, Wetting of flat and rough curved surfaces, J. Phys. Chem. C 113 (2009) 17275–17277, https://doi.org/10.1021/jp905237v.
[25] E.Y. Bormashenko, Physics of Wetting: Phenomena and Applications of Fluids On Surfaces, De Gruyter, Berlin, Boston, 2017, https://doi.org/10.1515/9783110444810.

[26] H. Qi, T. Wang, Z. Che, Air layer during the impact of droplets on heated substrates, Phys. Rev. E 101 (4) (2020), 043114, https://doi.org/10.1103/PhysRevE.101.043114.
[27] Q. Dai, M.M. Khonsari, C. Shen, W. Huang, X. Wang, Thermocapillary migration of liquid droplets induced by a unidirectional thermal gradient, Langmuir 32 (30) (2016) 7485–7492, https://doi.org/10.1021/acs.langmuir.6b01614.
[28] H. Linke, B.J. Alemán, L.D. Melling, M.J. Taormina, M.J. Francis, C.C. Dow-Hygelund, V. Narayanan, R.P. Taylor, A. Stout, Self-propelled leidenfrost droplets, Phys. Rev. Lett. 96 (15) (2006), 154502, https://doi.org/10.1103/PhysRevLett.96.154502.
[29] A. Gauthier, A. Bouillant, C. Clanet, D. Quéré, Aerodynamic repellency of impacting liquids, Phys. Rev. Fluid 3 (5) (2018), 054002, https://doi.org/10.1103/PhysRevFluids.3.054002.
[30] M. Taghilou, A. Salimi, Application of improved pseudo-potential model in examination of droplet dynamic on a rotary cylinder with high-density ratio, J. Mol. Liq. 290 (2019), 111240, https://doi.org/10.1016/j.molliq.2019.111240.
[31] Y. Couder, E. Fort, C.H. Gautier, A. Boudaoud, From bouncing to floating: noncoalescence of drops on a fluid bath, Phys. Rev. Lett. 94 (17) (2005), 177801, https://doi.org/10.1103/PhysRevLett.94.177801.
[32] Q. Dai, Z. Chong, W. Huang, X. Wang, Migration of liquid bridges at the interface of spheres and plates with an imposed thermal gradient, Langmuir 36 (22) (2020) 6268–6276, https://doi.org/10.1021/acs.langmuir.9b03951.
[33] P. García-Geijo, E.S. Quintero, G. Riboux, J.M. Gordillo, Spreading and splashing of drops impacting rough substrates, J. Fluid Mech. 917 (2021) A50, https://doi.org/10.1017/jfm.2021.313.
[34] W.Z. Yuan, L.Z. Zhang, Lattice boltzmann simulation of droplets impacting on superhydrophobic surfaces with randomly distributed rough structures, Langmuir 33 (3) (2017) 820–829, https://doi.org/10.1021/acs.langmuir.6b04041.
[35] J. Luo, S.Y. Wu, L. Xiao, Z.L. Chen, The maximum spreading lengths in circumferential and axial directions when droplets impact on cylindrical surfaces, Int. J. Multiph. Flow 143 (2021), 103774, https://doi.org/10.1016/j.ijmultiphaseflow.2021.103774.